arXiv:1410.5528v2 [cond-mat.soft] 23 Jan 2015

Structure and Osmotic Pressure of Ionic Microgel Dispersions

Mary M. Hedrick,[1,2] Jun Kyung Chung,[1,*] and Alan R. Denton[1,†]

[1] *Department of Physics, North Dakota State University, Fargo, ND 58108-6050, USA*
[2] *Department of Chemistry and Biochemistry, North Dakota State University, Fargo, ND 58108-6050, USA*

We investigate structural and thermodynamic properties of aqueous dispersions of ionic microgels – soft colloidal gel particles that exhibit unusual phase behavior. Starting from a coarse-grained model of microgel macroions as charged spheres that are permeable to microions, we perform simulations and theoretical calculations using two complementary implementations of Poisson-Boltzmann (PB) theory. Within a one-component model, based on a linear-screening approximation for effective electrostatic pair interactions, we perform molecular dynamics simulations to compute macroion-macroion radial distribution functions, static structure factors, and macroion contributions to the osmotic pressure. For the same model, using a variational approximation for the free energy, we compute both macroion and microion contributions to the osmotic pressure. Within a spherical cell model, which neglects macroion correlations, we solve the nonlinear PB equation to compute microion distributions and osmotic pressures. By comparing the one-component and cell model implementations of PB theory, we demonstrate that the linear-screening approximation is valid for moderately charged microgels. By further comparing cell model predictions with simulation data for osmotic pressure, we chart the cell model's limits in predicting osmotic pressures of salty dispersions.

I. INTRODUCTION

Microgels are colloidal gel particles, typically 10-1000 nm in size, dispersed in, and swollen by, a solvent. Since their first synthesis 65 years ago [1], microgel dispersions have drawn interdisciplinary interest that has grown at an accelerating pace over the past two decades [2]. Experimental and theoretical attention has been driven as much by fundamental interest in the unusual properties of these soft materials as by practical interest in potential applications. Recent reviews [3–6] describe prospective technologies, for example, in the chemical, biomedical, petroleum, and pharmaceutical industries.

Elastic, compressible, and interpenetrable gel particles can be highly sensitive to changes in solution conditions [7–12]. The degree of swelling can be controlled by adjusting temperature, pH, and chemical composition, including ionic strength. Extreme responsiveness of microgels to their environment often leads to unique mechanical and rheological properties, especially at concentrations near close packing [13–20], and makes microgels good candidates for chemical sensors and vehicles for targeted delivery and release of drugs [21–25].

In recent years, well-characterized dispersions of monodisperse microgels have been synthesized by emulsion polymerization and cross-linking of polyelectrolytes, such as poly(N-isopropylacrylamide) (PNIPAM) [26–28] or vinylpyridine [17]. The physical properties of polyelectrolyte microgel dispersions have been measured by a variety of experimental methods, including light scattering, small-angle neutron scattering, confocal microscopy, and osmometry, which have probed the connections between particle elasticity, osmotic pressure, structure, and phase behavior [29–39].

In water or other polar solvents, microgels become charged through dissociation of counterions from the polyelectrolyte backbones. The gel particles are then stabilized both sterically by dangling surface chains and electrostatically by electric charge. Because of their permeability to solvent molecules and small ions, and the prevalence of electrostatic forces, whose strength and range depend on degree of ionization and salt concentration, ionic microgels display unusual structural and thermodynamic properties [35, 40, 41] that are distinct from those of impermeable charged colloids [42].

Experimental advances have motivated related theoretical and computational modeling. Theoretical understanding of the swelling of bulk ionic networks (gels) has a long history [7–9, 43, 44]. More recent theoretical efforts have focused on effective electrostatic interactions between microgel macroions [45] and associated thermodynamic phase behavior [46]. For example, Gottwald *et al.* [47] calculated the phase diagram of dense dispersions of microgels governed by effective electrostatic interactions [45], using a powerful and elegant genetic algorithm to survey a wide variety of candidate crystal structures. Computer simulations of the primitive model [48, 49] and of coarse-grained bead-spring models of polyelectrolytes [48–51] have elucidated ion distributions and structure in dispersions of ionic microgels.

The present work is distinct from previous modeling studies in several respects. First, by focusing on significantly charged microgels, we highlight the influence of electrostatic interactions on bulk properties of ionic microgel dispersions. Second, we demonstrate several practical computational methods for modeling pair correlations and osmotic pressure, which are applicable also to other permeable macroions. Third, by comparing predictions of two alternative implementations of the Poisson-Boltzmann theory of polyelectrolyte solutions, we sys-

* Permanent address: Dongmyung School Corporation, 793 Tongil-ro Eunpyung-gu, Seoul, Republic of Korea
† Corresponding author: alan.denton@ndsu.edu

tematically assess the validity of perturbative theoretical approximations and of the widely used cell model.

The remainder of the paper is organized as follows. In Sec. II, we describe the physical models on which our simulations and calculations are based. Starting from the primitive model of polyelectrolytes and a uniform-sphere model of microgel macroions, we outline derivations of the one-component and cell models of ionic microgel dispersions. In Sec. III, we describe the computational methods – molecular dynamics simulation and thermodynamic perturbation theory – that we use to investigate physical properties of microgel dispersions. Details of the effective interactions required as input to the simulations and theory are deferred to the Appendix. In Sec. IV, we present numerical results for structural and thermodynamic properties, specifically the macroion-macroion radial distribution function, the static structure factor, and the equation of state (osmotic pressure vs. microgel density). Section V concludes with a summary of our main results and suggestions for future work.

II. MODELS

A. Primitive Model of Polyelectrolytes

Underlying our investigations is the primitive model of polyelectrolytes [52–54], which idealizes the solvent as a uniform medium. Applied to microgel dispersions, the model comprises spherical macroions and microions (counterions and salt ions) dispersed in a dielectric continuum, characterized only by a dielectric constant ϵ. Dissociation of counterions from polyelectrolyte chains and electrostatic screening are affected by pH and ionic strength. Here we assume constant pH and background ionic strength, thus fixing the macroion size and charge. For simplicity, we further assume that the macroions are monodisperse in radius a and valence Z and that their radius is independent of macroion concentration. The latter assumption is consistent with experiments, which indicate that crowding induces ionic microgel particles to de-swell only at concentrations approaching overlap [13].

Further abstracting, we treat the microions as monovalent point ions (valence $z = 1$). Bulk electroneutrality relates the macroion number N_m to the counterion and coion numbers $N_\pm$ via $ZN_m = N_+ - N_-$, assuming negative macroions. The total number of microions in the system can be expressed as $N_\mu = N_+ + N_- = ZN_m + 2N_s$, where $N_s = N_-$ is the number of salt ion pairs. Equivalently, the corresponding ion number densities are related via $Zn_m = n_+ - n_-$, $n_\mu = n_+ + n_-$, and $n_s = n_-$. The macroions are confined to a volume V, while the microions can exchange freely with an electrolyte reservoir of ion pair number density n_0 and bulk molar salt concentration $c_s^r = n_0/N_A$, where N_A is Avogadro's number. Donnan equilibrium between the system and reservoir generally leads to a salt concentration in the system $c_s = n_s/N_A$ that is lower than in the reservoir.

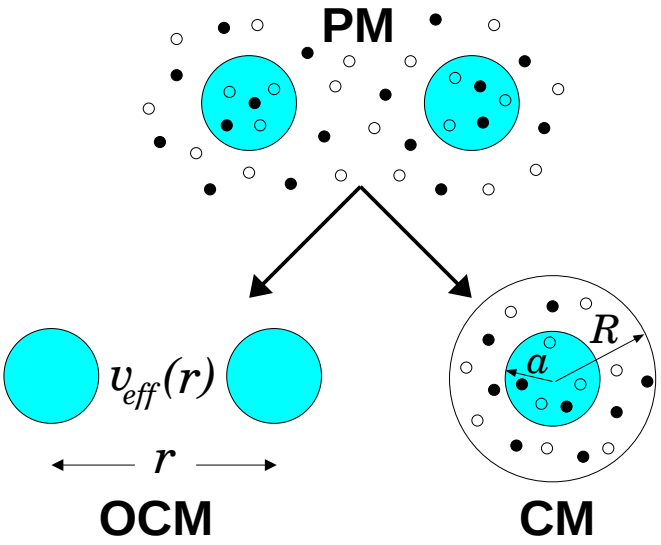

FIG. 1. The primitive model (PM) of ionic microgel dispersions comprises macroions (larger spheres) and explicit counterions and coions (smaller, light and dark spheres) dispersed in a uniform-dielectric solvent. The PM can be mapped onto either the coarse-grained one-component model (OCM), with implicit microions and pseudo-macroions interacting via an effective pair potential $v_{\rm eff}(r)$, or the cell model (CM), consisting of a single macroion centered in a spherical cell along with microions. In all models, the solution can exchange microions (in Donnan equilibrium) with an implicit salt reservoir.

The primitive model has a long tradition in predicting bulk properties of polyelectrolyte solutions [55] and charge-stabilized colloidal suspensions [42, 56, 57], including osmotic pressure and thermodynamic behavior. Nevertheless, neglect of molecular degrees of freedom, and thus all ion hydration effects, limits applications of the model to length scales much longer than the range of correlations between solvated ions. In the systems that we examine here, the Debye screening length, which characterizes the typical ion-ion correlation length, is at least 30 nm, justifying use of the primitive model.

B. Uniform-Sphere Model of Ionic Microgels

Spherical microgels, consisting of cross-linked networks of polyelectrolyte chains, typically vary in size from tens of nanometers to microns. When dispersed in water, the chains of ionic microgels (e.g., PNIPAM) can become charged through dissociation of protons or other oppositely charged counterions. The macroion size and charge may be adjusted by varying solution conditions (e.g., temperature and pH). The porous structure of the gel network allows water and microions to easily penetrate. Condensation (or close association) of some of the counterions can reduce the effective charge of ionic microgels, while bare Coulomb interactions between microgels are screened by mobile microions in solution.

The simplest model of an ionic microgel represents a macroion as a uniformly charged sphere, penetrable to microions, characterized by only a fixed charge number density $n_f = 3Z/(4\pi a^3)$ [45]. Neglecting the internal structure of the particle, this uniform-sphere model preserves the key properties of permeability and electrostatic screening, and is reasonable when the Debye screening length is much longer than the average distance between neighboring cross-links [44]. It should be noted, however, that the cross-link density distribution of real microgels depends on the chemical composition and mode of synthesis and can be nonuniform [58]. From Gauss's law, the electrostatic potential energy of a microion near a uniformly (negatively) charged spherical macroion is

$$\beta v_{m\mu}(r) \;=\; \begin{cases} -\dfrac{Zz\lambda_B}{r} \;, & r > a \\ -\dfrac{Zz\lambda_B}{2a}\left(3-\dfrac{r^2}{a^2}\right) \;, & r < a \;, \end{cases} \tag{1}$$

where $\beta \equiv 1/(k_BT)$ and $\lambda_B \equiv \beta e^2/\epsilon$ is the Bjerrum length – the distance at which two monovalent ions of charge e interact with the typical thermal energy k_BT at absolute temperature T. This macroion-microion interaction energy, along with the microion pair correlation functions, provides the essential input to the one-component model of ionic microgel dispersions with effective interactions.

C. One-Component Model of Microgel Dispersions

Interactions between ionic microgel macroions comprise an electrostatic component and a steric component associated with the elastic nature of the gel network. The electrostatic interactions are modeled here by an effective-interaction theory, previously developed by one of us [45, 59]. By formally integrating out the microion degrees of freedom from the partition function for the exact Hamiltonian of the multicomponent ion mixture, the theory maps the primitive model of the system onto a coarse-grained one-component model (OCM) governed by an *effective* Hamiltonian,

$$\mathcal{H}_{\rm eff} = K + E_0 + U(\mathbf{r}_1, \ldots, \mathbf{r}_{N_m}) \;. \tag{2}$$

The effective Hamiltonian includes the macroion kinetic energy K, a one-body volume energy E_0, which accounts for the microion free energy, and the internal potential energy $U(\{\mathbf{r}_i\})$ for macroions at positions $\mathbf{r}_i$ $(i = 1, \ldots, N_m)$. The volume energy – specified in the Appendix – while not affecting structural properties, does affect thermodynamic properties, such as pressure and phase stability.

In a linear-response approximation [60, 61], the microion densities respond linearly to the electrostatic potential of the macroions:

$$\hat{n}_\pm(\mathbf{k}) \;=\; \chi_\pm(k)\hat{v}_{m\pm}(k)\hat{n}_m(\mathbf{k}), \qquad k \neq 0 \;, \tag{3}$$

where $\hat{n}_\pm(\mathbf{k})$ are Fourier transforms (with wave vector $\mathbf{k}$) of the microion densities, $\chi_\pm(k)$ are linear response functions of a two-component microion plasma, and $\hat{v}_{m\pm}(k)$ are Fourier transforms of the macroion-microion electrostatic potential energy [Eq. (1)] for positive and negative $(z = \pm 1)$ microions. The $k \to 0$ limit must be treated separately, since the numbers of microions, $N_\pm = \hat{n}_\pm(0)$, do not respond to the macroion potential, but rather are determined by the electroneutrality constraint.

As described in detail elsewhere [45, 60, 61], the linear-response approximation [Eq. (3)], which is justified for sufficiently weak electrostatic coupling (typically, $Z\lambda_B/a < 5$), when combined with a mean-field random-phase approximation (RPA) for the microion response functions [60, 61], which is valid for weakly correlated monovalent $(z = 1)$ microions, yields the electrostatic potential inside and around a macroion (in units of k_BT/e):

$$\psi(r) \;=\; \begin{cases} \psi_>(r) \;, & r > a \\ \psi_<(r) \;, & r \le a \;, \end{cases} \tag{4}$$

with

$$\psi_>(r) \;=\; -\frac{3Z\lambda_B}{\tilde{\kappa}^2 r}\left(\cosh\tilde{\kappa} - \frac{\sinh\tilde{\kappa}}{\tilde{\kappa}}\right)e^{-\kappa r} \tag{5}$$

and

$$\psi_<(r) \;=\; -\frac{3Z\lambda_B}{\tilde{\kappa}^2 r}\left[\frac{r}{a} - \left(1+\frac{1}{\tilde{\kappa}}\right)e^{-\tilde{\kappa}}\sinh(\kappa r)\right] \;, \tag{6}$$

where $\kappa = \sqrt{4\pi\lambda_B n_\mu}$ is the screening constant in the system and $\tilde{\kappa} \equiv \kappa a$. The corresponding microion density profiles are

$$n_\pm(r) \;=\; n_\infty \mp n_\pm\psi(r) \;, \tag{7}$$

where $n_\infty = 2n_+n_+/n_\mu$.

Within the linear-response approximation, many-body effective interactions vanish and the internal potential energy can be expressed simply as a sum over macroion pairs of an effective pair potential $v_{\rm eff}(r_{ij})$:

$$U = \sum_{i<j=1}^{N_m} v_{\rm eff}(r_{ij}) \;, \tag{8}$$

where r_{ij} is the distance between the centers of macroions i and j. Within the mean-field approximation, the effective pair potential, which we take as input to molecular dynamics (MD) simulations and perturbation theory in Sec. III, can be expressed as [45]

$$v_{\rm eff}(r) \;=\; \begin{cases} v_{\rm Y}(r) \;, & r > 2a \\ v_{\rm ov} + v_{H}(r) \;, & r < 2a \;. \end{cases} \tag{9}$$

Nonoverlapping macroions interact via an effective Yukawa (screened-Coulomb) pair potential,

$$v_{\rm Y}(r) = A\frac{e^{-\kappa r}}{r}, \quad r > 2a \;, \tag{10}$$

with amplitude

$$\beta A = \lambda_B \left[\frac{3Z}{\tilde{\kappa}^2} \left(\cosh(\tilde{\kappa}) - \frac{\sinh \tilde{\kappa}}{\tilde{\kappa}} \right) \right]^2 . \qquad (11)$$

Overlapping macroions interact via a softer effective electrostatic pair potential $v_{\rm ov}(r)$ whose explicit form is given in the Appendix. For stronger electrostatic couplings ($Z\lambda_B/a > 5$), experience with charged colloids suggests that the Yukawa form of Eq. (10) may still hold, but with *renormalized* values for the parameters Z and κ [62–64].

Finally, the elastic repulsive interaction between the deformable cross-linked gel networks of a pair of contacting macroions we model by a Hertz potential [65]

$$v_{H}(r) = B \left(1 - \frac{r}{2a} \right)^{5/2} , \quad r < 2a , \qquad (12)$$

where the amplitude parameter B governs the strength of the repulsion. The phase diagram of Hertzian spheres was recently computed by Pàmies *et al.* [66] using Monte Carlo simulation. In the OCM, the total pressure,

$$p = p_{\rm id} + p_0 + p_m , \qquad (13)$$

decomposes naturally into a macroion ideal-gas term,

$$p_{\rm id} = n_m k_B T , \qquad (14)$$

a term associated with the microion volume energy,

$$p_0 = - \left(\frac{\partial E_0}{\partial V} \right)_{N_s/N_m} , \qquad (15)$$

an explicit expression for which is given in the Appendix, and a term due to effective interactions and correlations between macroion pairs,

$$p_m = - \left(\frac{\partial F_m}{\partial V} \right)_{N_s/N_m} , \qquad (16)$$

where F_m is the macroion contribution to the excess free energy. In Sec. IV, we calculate the macroion pressure from simulations and thermodynamic theory.

The theory of effective electrostatic interactions within the OCM, when coupled to the RPA for the microion linear-response functions, constitutes an implementation of the mean-field Poisson-Boltzmann (PB) theory. The chief appeal of this approach is its consistent inclusion of macroion-macroion interactions and correlations. Next, we review an alternative implementation of PB theory.

D. Cell Model of Microgel Dispersions

Another widespread implementation of PB theory is based on the cell model (CM). The principal advantages of this approach are its explicit incorporation of nonlinear microion screening and computational simplicity. Furthermore, comparisons between PB theory calculations within the CM for nanogels with uniform charge distribution and MD simulations of a more explicit bead-spring model demonstrate that the CM gives a reasonable representation of dilute, salt-free dispersions [49]. In Sec. IV A, we apply the CM to gauge the range of validity of the linear-screening approximation that underlies the effective pair potential employed in our simulations of the OCM. First, we briefly outline the CM, referring the reader to a thorough review for details [67].

Within the primitive model, the CM represents a bulk PE solution by a single macroion, confined to a cell of like shape together with explicit microions and a uniform dielectric solvent. Applied to ionic microgel dispersions, the CM places a macroion at the center of a spherical cell, of radius R determined by the macroion volume fraction $\phi = (a/R)^3$, along with a neutralizing number of counterions and coions, which can freely exchange with an electrolyte reservoir to maintain a fixed salt chemical potential (see Fig. 1). For simplicity, we assume here that the water within the macroion ($r < a$) has a dielectric constant equal to that of bulk water ($\epsilon \simeq 78$) at room temperature (Bjerrum length $\lambda_B = 0.7141$ nm), although experiments on ionic microgels indicate that the interior dielectric constant may be lower than in bulk [36, 68].

Combining the Poisson equation for the electrostatic potential $\varphi(r)$ with a Boltzmann approximation for the microion densities yields the nonlinear PB equation,

$$\psi''(r) + \frac{2}{r}\psi'(r) = \begin{cases} \kappa_0^2 \sinh \psi(r) + \dfrac{3Z\lambda_B}{a^3} , & 0 < r < a , \\ \kappa_0^2 \sinh \psi(r) , & a < r < R , \end{cases} \qquad (17)$$

where r is the radial distance from the center of the cell, $\psi(r) \equiv e\varphi(r)/k_BT$, and $\kappa_0 = \sqrt{8\pi\lambda_B n_0}$ is the screening constant in the salt reservoir. The mean-field Boltzmann approximation that underpins PB theory is equivalent to the RPA invoked in most applications of response theory and is similarly reasonable for weakly correlated monovalent microions.

The boundary conditions on Eq. (17) are as follows. Spherical symmetry and electroneutrality dictate that the electric field vanish at the cell center and boundary:

$$\psi'_{\rm in}(0) = 0 , \qquad \psi'_{\rm out}(R) = 0 , \qquad (18)$$

while continuity of the electrostatic potential and electric field at the microgel surface requires

$$\psi_{\rm in}(a) = \psi_{\rm out}(a) , \qquad \psi'_{\rm in}(a) = \psi'_{\rm out}(a) , \qquad (19)$$

the subscripts "in" and "out" labelling the solutions in the two regions. By numerically solving the PB equation [Eq. (17)], along with the boundary conditions [Eqs. (18) and (19)], we calculate the equilibrium microion distributions within the cell. In the process, we obtain the microion contribution to the pressure by applying the pressure theorem,

$$\beta p_\mu = n_+(R) + n_-(R) , \qquad (20)$$

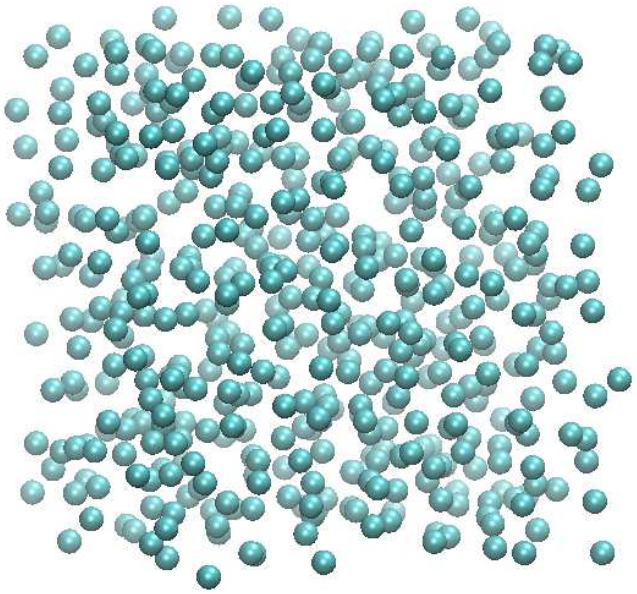

FIG. 2. Snapshot of an equilibrated fluid configuration of microgel particles from a molecular dynamics simulation.

which proves to be exact in the CM [55, 69]. The microion pressure p_μ in the CM is analogous to the volume pressure p_0 in the OCM [Eq. (15)].

III. COMPUTATIONAL METHODS

A. Molecular Dynamics Simulations

To explore the contribution of macroion interactions and correlations to the total pressure, we performed MD simulations, using LAMMPS [70], of microgel dispersions in the OCM. As input to the simulations, we used the effective pair potential described in Sec. II C and the Appendix. Exploiting the openness of the LAMMPS source code, we coded the microgel pair potential [Eq. (9)] as a new, customized class, supplementing the existing Yukawa pair potential class. In the canonical ensemble (constant N_m, V, T), we simulated $N_m = 4000$ macroions in a cubic box with periodic boundary conditions, initializing the particles on the sites of an fcc lattice and cutting off the long-range Yukawa potential at a radial distance of $r_c = 20/\kappa$. Comparisons of results from simulations of smaller systems ($N_m = 500$) confirmed that finite-size effects are negligible for $N_m = 4000$. After an initial equilibration period of 10^6 time steps, during which diagnostic quantities (energy, temperature, pressure) leveled off to stable plateaus, we collected statistics for 10^7 time steps. Figure 2 shows a typical snapshot from a simulation.

To compute the macroion contribution to the pressure from simulations of the OCM, we used the virial theorem. Generalized to density-dependent pair potentials [63, 71], this theorem states

$$p_m = \left\langle \frac{\mathcal{V}_{\rm int}}{3V} \right\rangle - \left\langle \left(\frac{\partial U}{\partial V} \right)_{N_s/N_m} \right\rangle + p_{\rm tail} \ , \qquad (21)$$

where $\mathcal{V}_{\rm int}$ denotes the internal virial, the volume derivative term accounts for the density dependence of the effective pair potential, angular brackets denote an ensemble average over configurations in the canonical ensemble, and $p_{\rm tail}$ corrects for cutting off the long-range tail of the pair potential. The internal virial is given by

$$\mathcal{V}_{\rm int} = \sum_{i=1}^{N_m} \mathbf{r}_i \cdot \mathbf{f}_i = \sum_{i<j=1}^{N_m} r_{ij} \mathrm{f}_{\rm eff}(r_{ij}) \ , \qquad (22)$$

where $\mathbf{f}_i$ is the effective force on macroion i due to all other macroions within a sphere of radius r_c and $\mathrm{f}_{\rm eff}(r_{ij}) = -v'_{\rm eff}(r_{ij})$ is the effective force exerted on macroion i by macroion j. For nonoverlapping macroion pairs, the effective Yukawa force is

$$\mathrm{f}_{\rm eff}(r_{ij}) = \left(\kappa + \frac{1}{r_{ij}} \right) v_{\rm eff}(r_{ij}) \ , \quad r_{ij} > 2a \ . \qquad (23)$$

An explicit expression for the effective electrostatic force between overlapping macroions is given in the Appendix.

The second term on the right side of Eq. (21) is computed, using Eq. (8), as the ensemble average of

$$\left(\frac{\partial U}{\partial V} \right)_{N_s/N_m} = -\frac{n_m}{V} \sum_{i<j=1}^{N_m} \left(\frac{\partial v_{\rm eff}(r_{ij})}{\partial n_m} \right)_{N_s/N_m} \ . \qquad (24)$$

For nonoverlapping macroion pairs, the effective Yukawa potential [Eq. (10)] yields

$$n_m \frac{\partial v_{\rm eff}(r)}{\partial n_m} = \left(\frac{\tilde{\kappa}^2 \sinh \tilde{\kappa}}{\tilde{\kappa} \cosh \tilde{\kappa} - \sinh \tilde{\kappa}} - 3 - \frac{\kappa r}{2} \right) v_{\rm eff}(r) \ . \qquad (25)$$

The corresponding expression for overlapping macroions is given in the Appendix.

Finally, the tail pressure is approximated by neglecting pair correlations beyond the cut-off radius, and thus setting $g(r) = 1$ for $r > r_c$, with the result

$$\begin{aligned} p_{\rm tail} &= -\frac{2\pi}{3} n_m^2 \int_{r_c}^{\infty} {\rm d}r \, r^3 v'_{\rm eff}(r) \\ &= \frac{2\pi}{3} n_m^2 \left(\frac{\kappa^2 r_c^2 + 3\kappa r_c + 3}{\kappa^2} \right) r_c v_{\rm eff}(r_c) \ , \end{aligned} \qquad (26)$$

where the integral is evaluated using the effective Yukawa pair potential.

B. Thermodynamic Perturbation Theory

To guide the choice of system parameters in our simulations, we adapt a thermodynamic theory previously

applied with success to charged colloids. The theory is based on a variational approximation [72–74] for the macroion excess free energy F_m, which combines first-order thermodynamic perturbation theory with a hard-sphere (HS) reference system:

$$f_m(n_m, n_s) = \min_{(d)} \left\{ f_{\rm HS}(n_m, n_s; d) + 2\pi n_m \int_d^\infty {\rm d}r\, r^2 g_{\rm HS}(r, n_m; d) v_{\rm eff}(r, n_m, n_s) \right\} . \quad (27)$$

Here $f_m = F_m/V$ is the macroion excess free energy density, $f_{\rm HS}$ and $g_{\rm HS}$ are, respectively, the excess free energy density and pair distribution function of the HS fluid, which we compute from the highly accurate Carnahan-Starling and Verlet-Weis expressions [74], and $v_{\rm eff}$ is the effective pair potential from Sec. III A. Minimization of f_m with respect to the effective HS diameter d yields a least upper bound to the free energy [74]. This perturbation theory is similar to previous implementations, with the exception that, in the present application to soft microgel macroions, it is possible for the effective hard-sphere diameter to be smaller than the macroion diameter ($d < 2a$).

In Donnan equilibrium, the salt concentration in the system is determined by imposing equality of salt chemical potentials between the system and reservoir. Treating the reservoir as an ideal gas of salt ions implies

$$\mu_s = 2k_BT \ln(n_0 \Lambda^3) \ , \quad (28)$$

where Λ is the de Broglie thermal wavelength and the system salt chemical potential is given by

$$\mu_s = \left(\frac{\partial}{\partial n_s} \frac{E_0 + F_m}{V} \right)_{n_m} . \quad (29)$$

An explicit expression can be found in the Appendix. From the macroion excess free energy, an approximation for the macroion-macroion interaction contribution to the total pressure follows immediately:

$$p_m = n_m^2 \left(\frac{\partial f_m}{\partial n_m} \right)_{N_s/N_m} , \quad (30)$$

which may be compared with the corresponding expression from the virial theorem [Eq. (21)]. In Sec. IV B, we apply this perturbation theory to calculate osmotic pressures of microgel dispersions.

IV. RESULTS AND DISCUSSION

A. One-Component Model vs. Cell Model

To explore thermodynamic and structural properties of ionic microgel dispersions, we implemented PB theory in the one-component and cell models. As described in Secs. II and III, we performed MD simulations and perturbation theory calculations in the OCM, and solved the nonlinear PB equation in the CM. Our choices of system parameters were guided by the recent experimental and modeling study of Riest *et al.* [35], who investigated structural properties of ionic microgel dispersions characterized by $a = 700$ nm, $Z = 150$, $\kappa a = 3.5$, and $B = 10^4\ k_BT$. Our simulations of this model system yielded radial distribution functions in agreement with ref. [35], although practically indistinguishable from those for uncharged ($Z = 0$) microgels dispersions, suggesting that electrostatic interactions in this relatively weakly coupled system ($Z\lambda_B/a \simeq 0.15$) are too weak to significantly influence pair structure.

To amplify electrostatic effects, we considered two representative model systems with increased valence or decreased size of microgels: (1) $a = 500$ nm, $Z = 1500$, c_s^r =10 μM, and (2) $a = 50$ nm, $Z = 100$, c_s^r =100 μM. We refer to these systems as "microgel" and "nanogel" dispersions, respectively. For both systems, we followed Riest *et al.* [35] in fixing the amplitude of the Hertz pair potential [Eq. (12)] at $B = 10^4\ k_BT$, corresponding to stiff elastic forces between contacting macroions. The chosen reservoir salt concentrations are low enough to yield relatively long Debye screening lengths – for microgels, $\kappa^{-1} \simeq 100$ nm ($\kappa a \simeq 5$), and for nanogels, $\kappa^{-1} \simeq 30$ nm ($\kappa a \simeq 1.7$). In such low-ionic-strength solutions, electrostatic interactions should significantly influence structural and thermodynamic properties.

According to their electrostatic coupling parameters, $Z\lambda_B/a \simeq 2.2$ and 1.4, both systems should still fall well within the linear-screening regime. To confirm this assumption, however, we first compare predictions of the linear-response and CM implementations of PB theory. Figures 3-6 show numerical results for the electrostatic potential, electric field, and microion number density profiles as functions of radial distance from the center of a macroion for two different microgel volume fractions. The results labeled OCM are calculated from the linear-response theory [Eq. (7)], while those labeled CM are calculated by solving the nonlinear PB equation [Eq. (17)] in a spherical cell. Although not expected to agree exactly, because of differing boundary conditions (free vs. cell) in the two implementations, the OCM and CM profiles are very similar, supporting the accuracy of the linearization approximation for these parameters. Comparison of results for $\phi = 0.01$ and 0.1 indicates weak sensitivity to geometrical artifacts of the CM.

Nonlinear screening may account for some part of the difference between the OCM and CM results, especially in the nanogel system, where a microion's electrostatic potential energy attains a larger fraction of the thermal energy within the macroion. In fact, solving the *linearized* PB equation does slightly alter the CM profiles, although care is needed in choosing a consistent reference potential around which to expand [64, 75]. As an extreme test of the linear-screening approximation, we also calculated $\psi(r)$ and $n_+(r)$ profiles for the parameters of

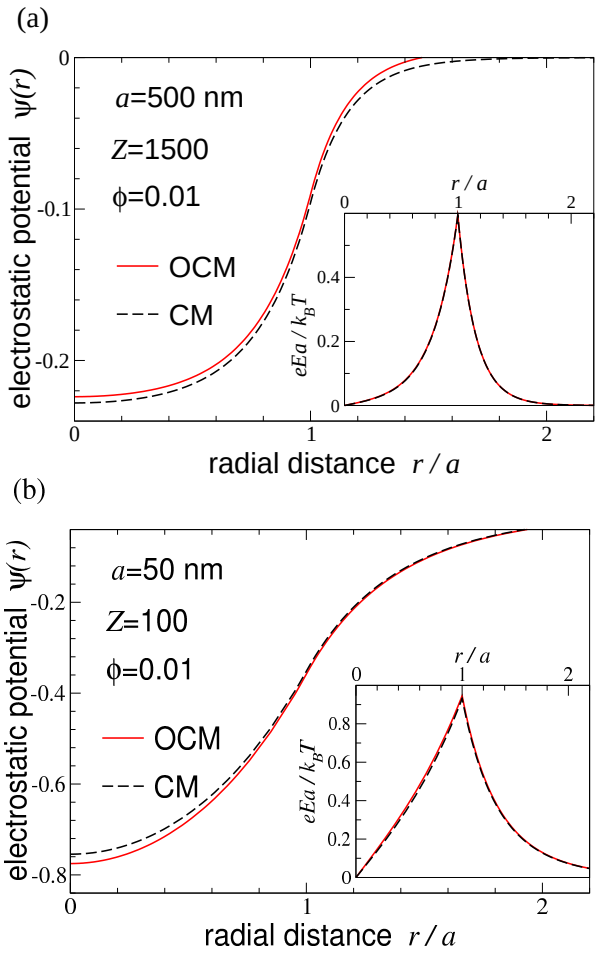

FIG. 3. Reduced electrostatic potential $\psi(r)$ and electric field $E(r)$ (inset) predicted by linear-response theory in one-component model (OCM, solid curves) and nonlinear PB theory in spherical cell model (CM, dashed curves). Results are shown for $\phi = 0.01$ volume fraction dispersions of (a) microgels: $a = 500$ nm, $Z = 1500$, $c_s^r = 10$ μM; and (b) nanogels: $a = 50$ nm, $Z = 100$, $c_s^r = 100$ μM. OCM $\psi(r)$ curves are offset to match CM curves at cell boundary ($r = R$).

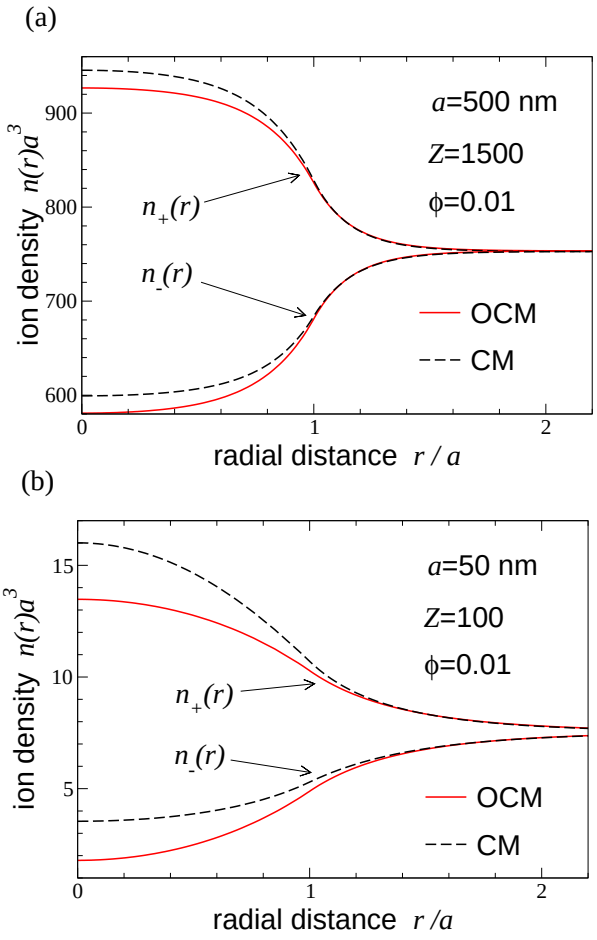

FIG. 4. Reduced microion number densities $n_\pm(r)$ predicted by linear-response theory in one-component model (OCM, solid curves) and nonlinear PB theory in spherical cell model (CM, dashed curves). Results are shown for dispersions of (a) microgels and (b) nanogels at volume fraction $\phi = 0.01$. System parameters are same as in Fig. 3.

ref. [49]: $a \simeq 10.6$ nm, $Z = 250$, $c_s^r = 0$. For this nanogel dispersion, we found that, compared with the CM, the OCM severely *underpredicts* the counterion density inside the microgel, verifying that this strongly-coupled system ($Z\lambda_B/a \simeq 17$) lies deep within the nonlinear regime.

B. Osmotic Pressure of Microgel Dispersions

Having demonstrated the accuracy of the linear-screening approximation for our system parameters, we proceed to input the effective pair potential [Eq. (9)] into both perturbation theory and MD simulations. Within each approach, we computed the osmotic pressure, defined as the difference in pressure between the system and the reservoir. To facilitate comparison, we omit here the common macroion ideal-gas contribution [Eq. (14)], defining the osmotic pressure for the two models as

$$\Pi = \begin{cases} p_0 + p_m - p_r & \text{(OCM)} \\ p_\mu - p_r & \text{(CM)} \ , \end{cases} \tag{31}$$

where $p_r = 2n_0 k_B T$ is the pressure of the (ideal-gas) reservoir. It should be noted that the volume pressure p_0 in the OCM, which is associated with the microion entropy and macroion-microion interaction energy, is comparable to, but distinct from, the microion pressure p_μ in the CM. Within the OCM, we computed the pressure from Eqs. (15) and (16), using the linear-screening approximation for the volume energy [Eqs. (A1)-(A3)]] and the variational approximation for the macroion free energy [Eq. (27)]. Within the CM, we computed the pressure from the pressure theorem [Eq. (20)].

Figure 7 presents a comparison between predictions of the OCM and the CM for the osmotic pressure vs. macroion volume fraction (equation of state). Although

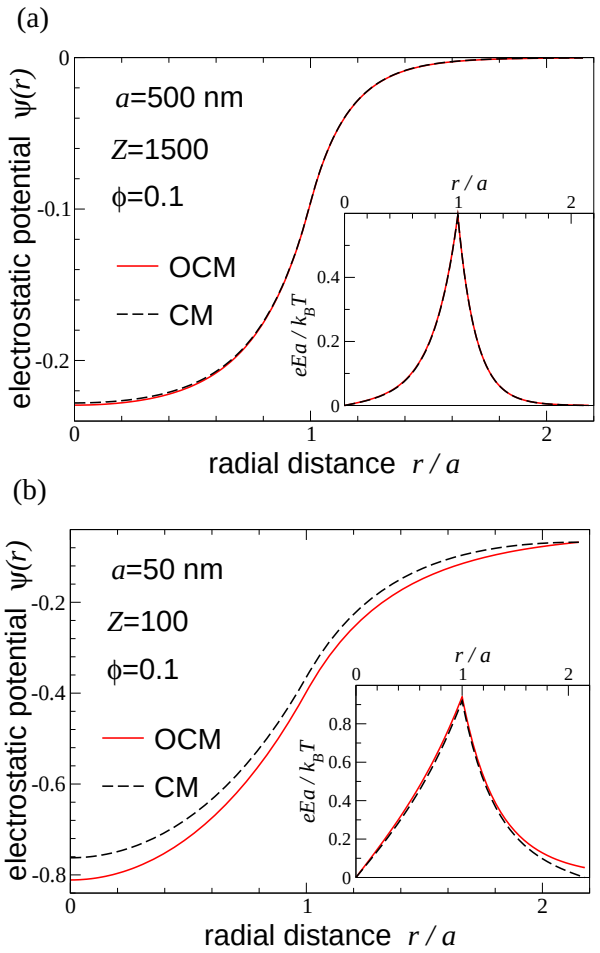

FIG. 5. Reduced electrostatic potential $\psi(r)$ and electric field $E(r)$ (inset) predicted by linear-response theory in one-component model (OCM, solid curves) and nonlinear PB theory in spherical cell model (CM, dashed curves). OCM $\psi(r)$ curves are offset to match CM curves at cell boundary ($r = R$). Results are shown for dispersions of (a) microgels and (b) nanogels at volume fraction $\phi = 0.1$. System parameters are same as in Fig. 3.

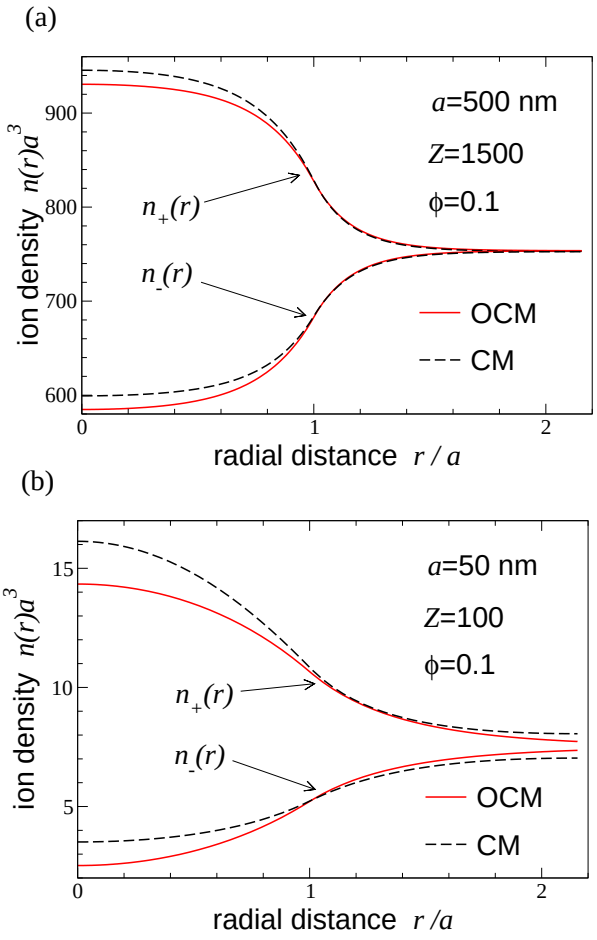

FIG. 6. Reduced microion number densities $n_{\pm}(r)$ predicted by linear-response theory in one-component model (OCM, solid curves) and nonlinear PB theory in spherical cell model (CM, dashed curves). Results are shown for dispersions of (a) microgels and (b) nanogels at volume fraction $\phi = 0.1$. System parameters are same as in Fig. 3.

the system salt concentrations – determined by equating salt chemical potentials [Eqs. (28) and (29)] in Donnan equilibrium – are nearly identical within the two models, the pressures differ significantly, especially so for the microgel system. Having ruled out geometry and nonlinear screening as significant sources of the discrepancy between predictions of the OCM and CM for these system parameters, we seek to isolate and examine the contribution to the pressure originating purely from macroion correlations, which the OCM includes but the CM neglects. To this end, as well as to test the accuracy of the variational approximation underlying the perturbation theory, we performed MD simulations, using the *same effective pair potential*, and computed the macroion pressure p_m essentially exactly (to within statistical error). Comparisons between predictions of perturbation theory for p_m and corresponding MD data are shown in Fig. 8.

Good agreement between predictions of perturbation theory and results of MD simulations demonstrates that the theory accurately models the macroion pressure. In fact, for the microgel system, the agreement is nearly exact over the whole range of concentrations considered. For the nanogel system, theory and simulation agree closely at lower volume fractions, while deviations emerge and grow for $\phi > 0.2$. Given that κa in the nanogel system is roughly 1/3 that in the microgel system, these deviations may reveal limitations of the perturbation theory when applied to such softly repulsive potentials. It is also noteworthy that the deviations coincide roughly with the onset of significant overlap of macroions, as reflected by the drop of the effective hard-sphere diameter below the bare macroion diameter ($d < 2a$) at $\phi \simeq 0.34$ (inset to Fig. 8(b)). The deviations may thus also signal the theory's limited ability to describe correlations between interpenetrating, soft particles.

Our analysis highlights the potentially important con-

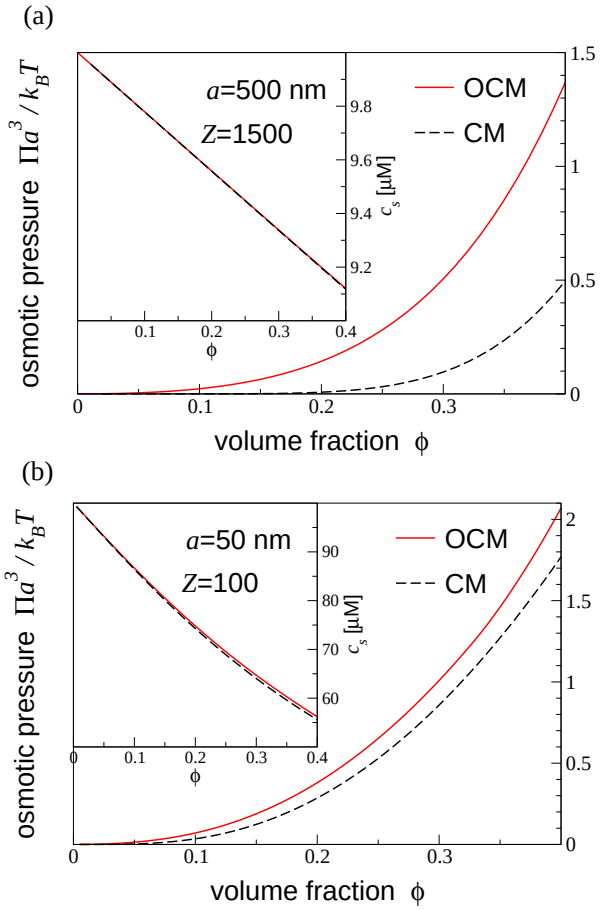

FIG. 7. Osmotic pressure [Eq. (31)] and salt concentration (insets) predicted by perturbation theory, with linearized effective interactions, in one-component model (OCM, solid) and nonlinear PB theory in spherical cell model (CM, dashed). Results are shown for dispersions of (a) microgels and (b) nanogels. System parameters are same as in Fig. 3.

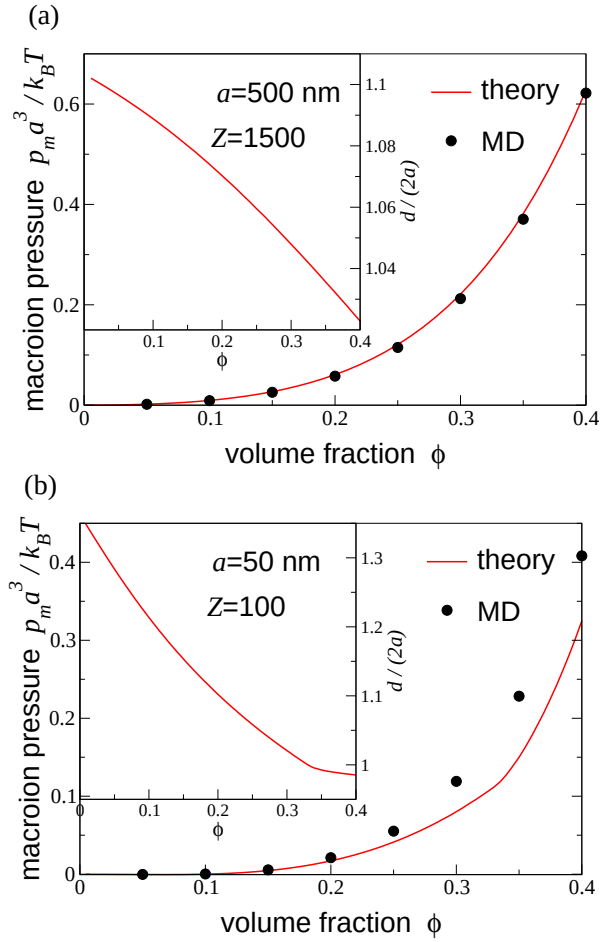

FIG. 8. Macroion contribution to total pressure from MD simulations (symbols) and perturbation theory (curves), both in one-component model with linearized effective interactions, for dispersions of (a) microgels and (b) nanogels. System parameters are same as in Fig. 3. Error bars on simulation data are smaller than symbol sizes. Insets show effective hard-sphere diameter d predicted by perturbation theory.

tribution of macroion correlations to the osmotic pressure of salty microgel dispersions. These results are consistent with recent studies revealing limitations of the cell model implementation of PB theory in predicting osmotic pressures of charge-stabilized colloidal suspensions [64, 76]. While the OCM, whose thermodynamic properties are accessible via simulations, perturbation theory, and integral-equation theories [35, 46, 74], naturally includes the full macroion contribution to the osmotic pressure, the CM entirely neglects the contribution due to macroion correlations, which can be significant at higher salt concentrations, where the microion contribution is relatively weak.

C. Structure of Microgel Dispersions

Beyond testing and confirming the accuracy of the perturbation theory for the macroion contribution to the osmotic pressure, simulations have the advantage of also providing insight into structure. To assess the significance of macroion correlations, we calculate structural properties from MD simulations of microgel dispersions. As an example, Fig. 9 shows results for the macroion-macroion radial distribution function $g(r)$ from our simulations of the OCM. Data are presented for both the microgel and nanogel systems, and represent averages over 10^4 configurations (coordinate sets), spaced by intervals of 10^3 time steps. We note that the hypernetted-chain (HNC) closure of the Ornstein-Zernike integral equation also yields very accurate results for these systems [35, 46].

With increasing concentration, as the macroion volume fraction increases from $\phi = 0.1$ to 0.4, the macroions evidently become more strongly correlated, as indicated by the growing height and narrowing width of the peaks. This trend confirms the significance of macroion correlations in these concentrated fluid dispersions. The precipitous drop of $g(r)$ near contact ($r = 2a$) indicates mini-

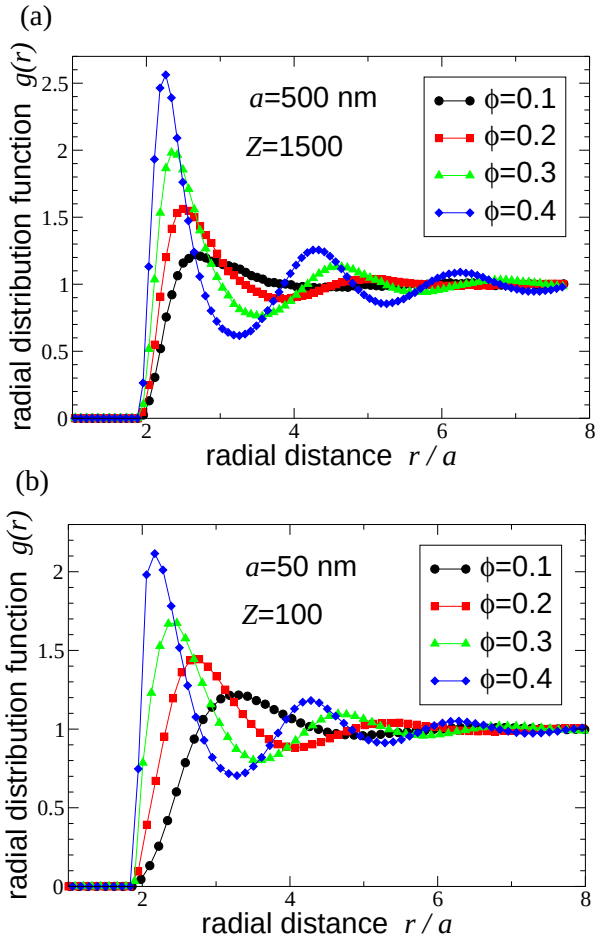

FIG. 9. Macroion-macroion radial distribution functions $g(r)$ from MD simulations of the OCM for dispersions of (a) microgels and (b) nanogels. System parameters are same as in Fig. 3. Radial distance r is in units of the macroion radius a. Error bars are smaller than symbol sizes. Curves are guides to the eye. Sharpening of peaks with increasing volume fraction ϕ reflects strengthening correlations between macroions.

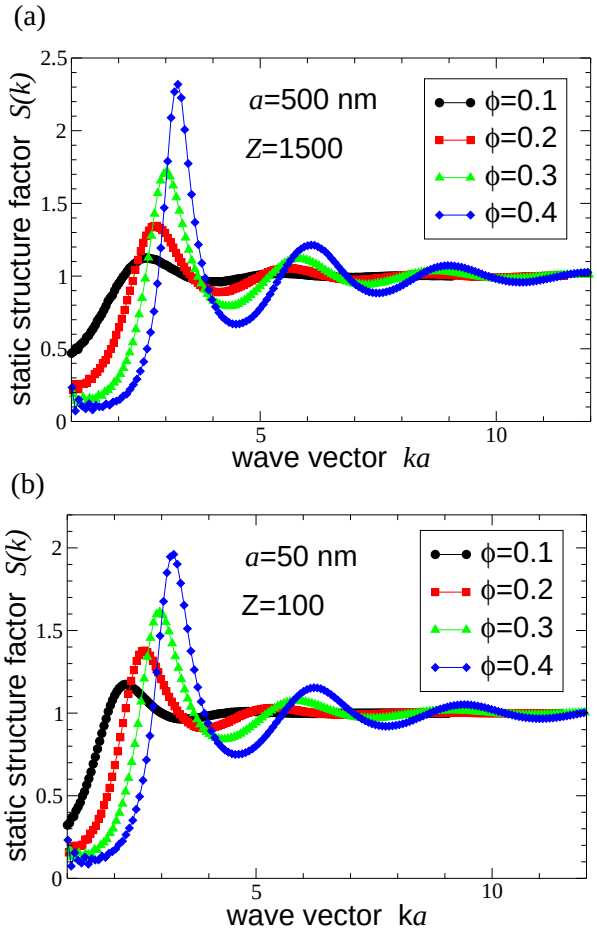

FIG. 10. Static structure factor $S(k)$ from MD simulations of the OCM for dispersions of (a) microgels and (b) nanogels, corresponding to radial distribution functions of Fig. 9. System parameters are same as in Fig. 3. Scattered wave vector magnitude k is in units of inverse macroion radius a^{-1}. Error bars are smaller than symbol sizes and curves are guides to the eye. Sharpening of peaks with increasing volume fraction ϕ reflects strengthening correlations between macroions.

mal deformation of macroions, as should be expected for such strongly repulsive (electrostatic and elastic) pair interactions. At the highest concentration considered here ($\phi = 0.4$), however, the nanogel macroions do interpenetrate up to a few percent of their diameter.

To complement our results for the radial distribution function, and to facilitate potential comparisons with scattering experiments, we also calculated the static structure factor, which is proportional to the Fourier transform of $g(r)$ and the intensity of scattered radiation (light, X-rays, neutrons). For a uniform, isotropic fluid, the static structure factor can be defined as

$$S(k) = \frac{2}{N_m} \sum_{i<j=1}^{N_m} \left\langle \frac{\sin(kr_{ij})}{kr_{ij}} \right\rangle + 1 \ , \qquad (32)$$

where k is the magnitude of the scattered wave vector. In practice, we calculate $S(k)$ from averages over the same configurations used to compute $g(r)$. Although we make no attempt here to accurately calculate the long-wavelength ($k \to 0$) limit of $S(k)$, techniques to correct for finite-size effects could be applied if needed [77, 78].

Figure 10 shows our results for the static structure factor corresponding to the radial distribution functions in Fig. 9. As with the $g(r)$ data, sharpening of the peaks in $S(k)$ with increasing macroion concentration reflects strengthening correlations between macroions. These correlations, omitted from the CM, can significantly influence the bulk osmotic pressure of salty dispersions in the fluid state [64, 76], as shown above in Sec. IV B.

At sufficiently high volume fractions, or low salt concentrations, where the Debye screening length κ^{-1} substantially exceeds the average nearest-neighbor separation, $\bar{d} \sim a(\phi^{-1/3} - 1)$, a solid phase may be stabilized. In this limit, the CM proves accurate, if only because,

under these conditions, the microion contribution to the osmotic pressure dominates the macroion contribution. For impenetrable charged colloids, the analysis of Hallez *et al.* [76] shows that, for moderately coupled systems ($Z\lambda_B/a < 8$), the CM is generally reliable for $\kappa\bar{d} < 1$. Although a similar analysis is yet to be performed for penetrable macroions, it is worth noting that our microgel system straddles the threshold, $\kappa\bar{d} \simeq 1$, while our nanogel system lies well beyond the range of accuracy of the CM ($\kappa\bar{d} > 1$).

V. CONCLUSIONS

In summary, we have investigated thermodynamic and structural properties of ionic microgels – modeled as soft, uniformly charged spheres – dispersed in salty solutions with monovalent microions, using Poisson-Boltzmann theory and molecular dynamics simulation. We implemented PB theory within two derivatives of the primitive model: (1) a one-component model, with effective pair interactions between microgels, and (2) a cell model, focused on a single microgel. In the OCM, we invoked a linear-screening approximation for effective electrostatic interactions, which we input into both MD simulations and a thermodynamic perturbation theory based on a variational approximation for the free energy. In the CM, we numerically solved the nonlinear PB equation in a spherical cell geometry.

For two model systems ranging from nanogels to microgels, with moderate electrostatic coupling strengths ($1 < Z\lambda_B/a < 3$), the linear and nonlinear implementations of PB theory predict very similar microion distributions, justifying the linear-screening approximation assumed within the OCM. For these systems, perturbation theory and MD simulations – based on the same effective pair potentials – agree closely for the macroion contribution to the pressure, quantitative deviations emerging only for dense dispersions of interpenetrating particles with relatively long-range repulsive interactions. This agreement validates the variational approximation, at least for non-penetrating particles with short-range repulsive interactions.

Our calculations of osmotic pressure demonstrate that macroion interactions and correlations can make an important contribution to the total pressure of ionic microgel dispersions, even at relatively low (sub-mM) salt concentrations. The significance of macroion correlations in our model systems is confirmed by our MD analysis, which reveals that macroion-macroion radial distribution functions and static structure factors are highly structured in concentrated dispersions. We conclude that the coarse-grained OCM provides a computationally practical framework for exploring physical properties of ionic microgel dispersions and that the PB cell model, while reliable when applied to deionized solutions, should be applied with caution to salty solutions, as was demonstrated previously for charged colloids [64, 76].

In the future, it will be important to test predictions of the OCM for thermodynamic and structural properties against results from experiments and from simulations of the primitive model, which explicitly include microions. Previous such comparisons for charged colloids [62–64] have charted the range of accuracy of the OCM for impenetrable particles, identified the threshold for the onset of nonlinear screening effects, and helped to test and calibrate charge-renormalization theories. Similar comparisons for ionic microgels would help to motivate development of renormalization theories for dispersions of more strongly coupled (highly charged) penetrable particles [49]. Such a comprehensive theory would help to guide further exploration of the bulk modulus and phase stability of ionic microgel dispersions. Future work may also extend the methods described here to microgels with nonuniform fixed charge distributions, such as core-shell particles, and to other soft ionic colloids, such as polyelectrolyte stars, dendrites, and microcapsules [79].

ACKNOWLEDGMENTS

We thank Qiyun Tang and Brandon J. Johnson for helpful discussions. This work was supported by the National Science Foundation (Grant No. DMR-1106331). MMH thanks the McNair Scholars Program for support.

Appendix A: Effective Interaction Theory

In the linear-screening approximation [45] for the uniform-sphere model of microgels, the volume energy per macroion is given by

$$\frac{\beta E_0}{N_m} = \frac{\beta F_p}{N_m} - 3Z^2\frac{\lambda_B}{a}\left\{\frac{1}{5} - \frac{1}{2\tilde{\kappa}^2} + \frac{3}{4\tilde{\kappa}^3}\left[1 - \frac{1}{\tilde{\kappa}^2} + \left(1 + \frac{2}{\tilde{\kappa}} + \frac{1}{\tilde{\kappa}^2}\right)e^{-2\tilde{\kappa}}\right]\right\} - \frac{Z}{2}\frac{n_+ - n_-}{n_+ + n_-}\,, \quad \text{(A1)}$$

where $\tilde{\kappa} \equiv \kappa a$ and the microion plasma free energy,

$$\beta F_p \;=\; N_+[\ln(n_+\Lambda^3) - 1] \;+\; N_-[\ln(n_-\Lambda^3) - 1]\,, \quad \text{(A2)}$$

is the free energy of an ideal gas of microions in a uniform compensating background. The corresponding volume pressure [Eq. (15)] is given by

$$\beta p_0 = n_\mu + \frac{3}{2}Z^2\frac{\lambda_B}{a}n_m\left[-\frac{1}{\tilde{\kappa}^2} + \frac{9}{4\tilde{\kappa}^3} - \frac{15}{4\tilde{\kappa}^5} + \left(\frac{3}{2\tilde{\kappa}^2} + \frac{21}{4\tilde{\kappa}^3} + \frac{15}{2\tilde{\kappa}^4} + \frac{15}{4\tilde{\kappa}^5}\right)e^{-2\tilde{\kappa}}\right]\,, \quad \text{(A3)}$$

and the system salt chemical potential [Eq. (29)] by

$$\beta\mu_s = \beta\left(\frac{\partial f_m}{\partial n_s}\right)_{n_m} + \ln(n_+\Lambda^3) + \ln(n_-\Lambda^3) + \frac{Zn_m}{n_\mu^2} + 3Z^2\frac{\lambda_B}{a}\frac{n_m}{n_\mu}\left[-\frac{1}{\tilde{\kappa}^2} + \frac{9}{4\tilde{\kappa}^3} - \frac{15}{4\tilde{\kappa}^5} + \left(\frac{3}{2\tilde{\kappa}^2} + \frac{21}{4\tilde{\kappa}^3} + \frac{15}{2\tilde{\kappa}^4} + \frac{15}{4\tilde{\kappa}^5}\right)e^{-2\tilde{\kappa}}\right] . \quad \text{(A4)}$$

The effective electrostatic pair potential between overlapping macroions is

$$v_{\rm ov}(r) = v_{mm}(r) + v_{\rm ind}(r) , \quad r < 2a , \quad \text{(A5)}$$

where

$$\beta v_{mm}(r) = Z^2\frac{\lambda_B}{a}\left(\frac{6}{5} - \frac{1}{2}\tilde{r}^2 + \frac{3}{16}\tilde{r}^3 - \frac{1}{160}\tilde{r}^5\right) \quad \text{(A6)}$$

is the bare (Coulomb) pair potential between two overlapping, uniformly charged spheres and

$$\beta v_{\rm ind}(r) = -\left(\frac{3Z}{\tilde{\kappa}^2}\right)^2\frac{\lambda_B}{2r}\left[\left(1+\frac{1}{\tilde{\kappa}}\right)^2 e^{-2\tilde{\kappa}}\sinh(\kappa r) + \left(1-\frac{1}{\tilde{\kappa}^2}\right)\left(1 - e^{-\kappa r} + \frac{1}{2}\kappa^2 r^2 + \frac{1}{24}\kappa^4 r^4\right) - \frac{2}{3}\tilde{\kappa}^2\left(1-\frac{2}{5}\tilde{\kappa}^2\right)\tilde{r} - \frac{1}{9}\tilde{\kappa}^4\tilde{r}^3 - \frac{1}{720}\tilde{\kappa}^4\tilde{r}^6\right] \quad \text{(A7)}$$

is the microion-induced pair potential, where $\tilde{r} \equiv r/a$. The corresponding effective electrostatic force between a pair of overlapping macroions is given by

$$\mathrm{f}_{\rm ov}(r) = -v'_{\rm ov}(r) = \mathrm{f}_{mm}(r) + \mathrm{f}_{\rm ind}(r) , \quad \text{(A8)}$$

where

$$\beta\mathrm{f}_{mm}(r) = Z^2\frac{\lambda_B}{a^2}\left(\tilde{r} - \frac{9}{16}\tilde{r}^2 + \frac{1}{32}\tilde{r}^4\right) \quad \text{(A9)}$$

is the bare electrostatic force and

$$\beta\mathrm{f}_{\rm ind}(r) = \left(\frac{3Z}{\tilde{\kappa}}^2\right)^2\frac{\kappa\lambda_B}{2r}\left[\left(1+\frac{1}{\tilde{\kappa}}\right)^2 e^{-2\tilde{\kappa}}\cosh(\kappa r) + \left(1-\frac{1}{\tilde{\kappa}^2}\right)\left(e^{-\kappa r} + \kappa r + \frac{1}{6}\kappa^3 r^3\right) - \frac{2}{3}\tilde{\kappa}\left(1-\frac{2}{5}\tilde{\kappa}^2\right) - \frac{1}{3}\tilde{\kappa}^3\tilde{r}^2 - \frac{1}{120}\tilde{\kappa}^3\tilde{r}^5\right] + \frac{\beta v_{\rm ind}(r)}{r} \quad \text{(A10)}$$

is the microion-induced electrostatic force.

Finally, the density derivative of the effective electrostatic pair potential between overlapping macroions, which appears in Eq. (24), is given by

$$n_m\left(\frac{\partial v_{\rm eff}(r)}{\partial n_m}\right)_{N_s/N_m} = \frac{\kappa}{2}\left(\frac{\partial v_{\rm eff}(r)}{\partial\kappa}\right) \quad \text{(A11)}$$

with

$$\beta\left(\frac{\partial v_{\rm eff}(r)}{\partial\kappa}\right) = -\left(\frac{3Z}{\tilde{\kappa}^2}\right)^2\frac{\lambda_B}{2r}\left[-2 + \tilde{r}^2 + \frac{3}{\tilde{\kappa}^2} + \frac{2}{3}\tilde{\kappa}^2\tilde{r} - \frac{1}{2}\tilde{\kappa}^2\tilde{r}^2 + \frac{1}{24}\tilde{\kappa}^2\tilde{r}^4 + \left(2 + \frac{\kappa r}{2} - \frac{3}{\tilde{\kappa}^2} - \frac{\tilde{r}}{2\tilde{\kappa}}\right)e^{-\kappa r} - \left(4 + \tilde{\kappa} + \frac{6}{\tilde{\kappa}} + \frac{3}{\tilde{\kappa}^2}\right)e^{-2\tilde{\kappa}}\sinh(\kappa r) + \frac{1}{2}\left(1+\frac{1}{\tilde{\kappa}}\right)^2 e^{-2\tilde{\kappa}}\kappa r\cosh(\kappa r)\right] . \quad \text{(A12)}$$

[1] W. O. Baker, Ind. Eng. Chem. **41**, 511 (1949).
[2] *Web of Science* (Thomson Reuters, 2014).
[3] L. A. Lyon and A. Fernández-Nieves, Annu. Rev. Phys. Chem. **63**, 25 (2012).
[4] L. A. Lyon and M. J. Serpe, eds., *Hydrogel Micro and Nanoparticles* (Wiley-VCH Verlag GmbH & Co. KGaA, Weinheim, 2012).
[5] A. Fernández-Nieves, H. Wyss, J. Mattsson, and D. A. Weitz, eds., *Microgel Suspensions: Fundamentals and Applications* (Wiley-VCH Verlag GmbH & Co. KGaA, Weinheim, 2011).
[6] R. H. Pelton, Adv. Colloid Interface Sci. **85**, 1 (2000).
[7] P. J. Flory, *Principles of Polymer Chemistry* (Cornell University Press, Ithaca, 1953).
[8] A. Katchalsky, S. Lifson, and H. Eisenberg, J. Polym. Sci. A **7**, 571 (1951).
[9] A. Katchalsky and I. Michaeli, J. Polym. Sci. A **15**, 69 (1955).
[10] G. Romeo and M. P. Ciamarra, Soft Matter **9**, 5401 (2013).
[11] J. J. Liétor-Santos, B. Sierra-Martín, and A. Fernández-Nieves, Phys. Rev. E **84**, 060402(R) (2011).
[12] P. Menut, S. Seiffert, J. Sprakel, and D. A. Weitz, Soft Matter **8**, 156 (2012).
[13] A. Fernández-Nieves, A. Fernández-Barbero, B. Vincent, and F. J. de las Nieves, J. Chem. Phys. **119**, 10383 (2003).
[14] J. J. Liétor-Santos, B. Sierra-Martín, R. Vavrin, Z. Hu, U. Gasser, and A. Fernández-Nieves, Macromol. **42**, 6225 (2009).
[15] S. M. Hashmi and E. R. Dufresne, Soft Matter **5**, 3682 (2009).

[16] J. J. Liétor-Santos, U. Gasser, R. Vavrin, Z. B. Hu, and A. Fernández-Nieves, J. Chem. Phys. **133**, 034901 (2010).

[17] B. Sierra-Martín, Y. Laporte, A. B. South, L. A. Lyon, and A. Fernández-Nieves, Phys. Rev. E **84**, 011406 (2011).

[18] J. J. Liétor-Santos, B. Sierra-Martín, U. Gasser, and A. Fernández-Nieves, Soft Matter **7**, 6370 (2011).

[19] G. Romeo, L. Imperiali, J.-W. Kim, A. Fernández-Nieves, and D. A. Weitz, J. Chem. Phys. **136**, 124905 (2012).

[20] A. Bouchoux, P. Qu, P. Bacchin, and G. Gésan-Guiziou, Langmuir **30**, 22 (2013).

[21] M. Hamidi, A. Azadi, and P. Rafiei, Advanced Drug Delivery Reviews **60**, 1638 (2008).

[22] J. K. Oh, R. Drumright, D. J. Siegwart, and K. Matyjaszewski, Prog. Polym. Sci. **33**, 448 (2008).

[23] J. K. Oh, D. I. Lee, and J. M. Park, Progress in Polymer Science **34**, 1261 (2009).

[24] S. Schmidt, P. A. L. Fernandes, B. G. D. Geest, M. Delcea, A. G. Skirtach, H. Möhwald, and A. Fery, Adv. Funct. Mater. **21**, 1411 (2011).

[25] D. Sivakumaran, D. Maitland, T. Oszustowicz, and T. Hoare, J. Colloid Interface Sci. **392**, 422 (2013).

[26] R. H. Pelton and P. Chibante, Colloids Surf. **20**, 247 (1986).

[27] R. K. Shah, J.-W. Kim, J. J. Agresti, D. A. Weitz, and L.-Y. Chu, Soft Matter **4**, 2303 (2008).

[28] T. Still, K. Chen, A. M. Alsayed, K. B. Aptowicz, and A. G. Yodh, J. Colloid Interface Sci. **405**, 96 (2013).

[29] H. Senff and W. Richtering, J. Phys. Chem. **111**, 1705 (1999).

[30] J. Wu, G. Huang, and Z. Hu, Macromol. **36**, 440 (2003).

[31] T. Eckert and W. Richtering, J. Chem. Phys. **129**, 124902 (2008).

[32] A. N. St. John, V. Breedveld, and L. A. Lyon, J. Phys. Chem. B **111**, 7796 (2007).

[33] M. Muluneh and D. A. Weitz, Phys. Rev. E **85**, 021405 (2012).

[34] B. Sierra-Martín and A. Fernández-Nieves, Soft Matter **8**, 4141 (2012).

[35] J. Riest, P. Mohanty, P. Schurtenberger, and C. N. Likos, Z. Phys. Chem. **226**, 711 (2012).

[36] P. S. Mohanty, A. Yethiraj, and P. Schurtenberger, Soft Matter **8**, 10819 (2012).

[37] D. Paloli, P. S. Mohanty, J. J. Crassous, E. Zaccarelli, and P. Schurtenberger, Soft Matter **9**, 3000 (2013).

[38] U. Gasser, J.-J. Liétor-Santos, A. Scotti, O. Bunk, A. Menzel, and A. Fernández-Nieves, Phys. Rev. E **88**, 052308 (2013).

[39] P. S. Mohanty, D. Paloli, J. J. Crassous, E. Zaccarelli, and P. Schurtenberger, J. Chem. Phys. **140**, 094901 (2014).

[40] F. Gröhn and M. Antonietti, Macromol. **33**, 5938 (2000).

[41] A. Fernández-Nieves and M. Márquez, J. Chem. Phys. **122**, 084702 (2005).

[42] P. N. Pusey, "Colloidal suspensions," in *Liquids, Freezing and Glass Transition, Les Houches session 51*, Vol. 2, edited by J.-P. Hansen, D. Levesque, and J. Zinn-Justin (North-Holland, Amsterdam, 1991) pp. 763–931.

[43] P.-G. de Gennes, *Scaling Concepts in Polymer Physics* (Cornell, Ithaca, 1979).

[44] J.-L. Barrat, J.-F. Joanny, and P. Pincus, J. Phys. II France **2**, 1531 (1992).

[45] A. R. Denton, Phys. Rev. E **67**, 011804 (2003), **68**, 049904(E) (2003).

[46] C. N. Likos, in *Microgel Suspensions: Fundamentals and Applications*, edited by A. Fernández-Nieves, H. Wyss, J. Mattsson, and D. A. Weitz (Wiley-VCH Verlag GmbH & Co. KGaA, Weinheim, 2011) pp. 165–193.

[47] D. Gottwald, C. N. Likos, G. Kahl, and H. Löwen, J. Chem. Phys. **122**, 074903 (2005).

[48] S. Schneider and P. Linse, Eur. Phys. J. E **8**, 457 (2002).

[49] G. C. Claudio, K. Kremer, and C. Holm, J. Chem. Phys. 131 **131**, 094903 (2009).

[50] M. Quesada-Pérez and A. Martín-Molina, Soft Matter **9**, 7086 (2013).

[51] H. Kobayashi and R. G. Winkler, Polymers **6**, 1602 (2014).

[52] F. Oosawa, *Polyelectrolytes* (Dekker, New York, 1971).

[53] M. Doi and S. F. Edwards, *The Theory of Polymer Dynamics* (Clarendon, Oxford, 1988).

[54] M. Hara, ed., *Polyelectrolytes* (Dekker, New York, 1993).

[55] R. A. Marcus, J. Chem. Phys. **23**, 1057 (1955).

[56] B. V. Derjaguin and L. Landau, Acta Physicochimica **14**, 633 (1941).

[57] E. J. W. Verwey and J. T. G. Overbeek, *Theory of the Stability of Lyophobic Colloids* (Elsevier, Amsterdam, 1948).

[58] T. Hoare and D. McLean, J. Phys. Chem. B **110**, 20327 (2006).

[59] A. R. Denton, "Effective interactions in soft materials," in *Nanostructured Soft Matter: Experiment, Theory, Simulation and Perspectives*, edited by A. V. Zvelindovsky (Springer, 2007) pp. 395–433.

[60] A. R. Denton, J. Phys.: Condens. Matter **11**, 10061 (1999).

[61] A. R. Denton, Phys. Rev. E **62**, 3855 (2000).

[62] A. R. Denton, J. Phys.: Condens. Matter **20**, 494230 (2008).

[63] B. Lu and A. R. Denton, Commun. Comp. Phys. **7**, 235 (2010).

[64] A. R. Denton, J. Phys.: Condens. Matter **22**, 364108 (2010).

[65] L. D. Landau and E. M. Lifshitz, *Theory of Elasticity*, 3rd ed. (Elsevier, Amsterdam, 1986).

[66] J. C. Pàmies, A. Cacciuto, and D. Frenkel, J. Chem. Phys. **131**, 044514 (2009).

[67] M. Deserno and C. Holm, in *Electrostatic Effects in Soft Matter and Biophysics*, NATO Advanced Studies Institute, Series II: Mathematics Physics and Chemistry, Vol. 46, edited by C. Holm, P. Kékicheff, and R. Podgornik (Kluwer, Dordrecht, 2001) pp. 27–50.

[68] M. Parthasarathy and D. Klingenberg, Mater. Sci. Eng. **R17**, 57 (1996).

[69] H. Wennerström, B. Jönsson, and P. Linse, J. Chem. Phys. **76**, 4665 (1982).

[70] S. Plimpton, J. Comp. Phys. **117**, 1 (1995).

[71] A. A. Louis, J. Phys.: Condens. Matter **14**, 9187 (2002).

[72] R. van Roij and J. P. Hansen, Phys. Rev. Lett. **79**, 3082 (1997).

[73] A. R. Denton, Phys. Rev. E **73**, 041407 (2006).

[74] J.-P. Hansen and I. R. McDonald, *Theory of Simple Liquids*, 3rd ed. (Elsevier, London, 2006).

[75] M. Deserno and H. H. von Grünberg, Phys. Rev. E **66**, 011401 (2002).

[76] Y. Hallez, J. Diatta, and M. Meireles, Langmuir **30**, 6721 (2014).

[77] J. J. Salacuse, A. R. Denton, and P. A. Egelstaff, Phys.

Rev. E **53**, 2382 (1996).
[78] J. J. Salacuse, A. R. Denton, P. A. Egelstaff, M. Tau, and L. Reatto, Phys. Rev. E **53**, 2390 (1996).
[79] Q. Tang and A. R. Denton, Phys. Chem. Chem. Phys. **16**, 20924 (2014).